

TRANSFORMER MEETS TWICING: HARNESSING UNATTENDED RESIDUAL INFORMATION

Anonymous authors

Paper under double-blind review

ABSTRACT

Transformer-based deep learning models have achieved state-of-the-art performance across numerous language and vision tasks. While the self-attention mechanism, a core component of transformers, has proven capable of handling complex data patterns, it has been observed that the representational capacity of the attention matrix degrades significantly across transformer layers, thereby hurting its overall performance. In this work, we leverage the connection between self-attention computations and low-pass non-local means (NLM) smoothing filters and propose the Twicing Attention, a novel attention mechanism that uses *kernel twicing procedure* in nonparametric regression to alleviate the low-pass behavior of associated NLM smoothing with compelling theoretical guarantees and enhanced adversarial robustness. This approach enables the extraction and reuse of meaningful information retained in the residuals following the imperfect smoothing operation at each layer. Our proposed method offers two key advantages over standard self-attention: 1) a provably slower decay of representational capacity and 2) improved robustness and accuracy across various data modalities and tasks. We empirically demonstrate the performance gains of our model over baseline transformers on multiple tasks and benchmarks, including image classification and language modeling, on both clean and corrupted data.

1 INTRODUCTION

Attention mechanisms and transformers (Vaswani et al., 2017) have achieved state of the art performance across a wide variety of tasks in machine learning (Khan et al., 2022; Lin et al., 2022; Tay et al., 2022) and, in particular, within natural language processing (Al-Rfou et al., 2019; Baevski & Auli, 2018; Dehghani et al., 2018; Raffel et al., 2020; Dai et al., 2019), computer vision (Liu et al., 2021; Touvron et al., 2021; Radford et al., 2021), and reinforcement learning (Janner et al., 2021; Chen et al., 2021). They have also demonstrated strong performance in knowledge transfer from pretraining tasks to various downstream tasks with weak or no supervision (Radford et al., 2018; 2019; Devlin et al., 2018). At the core of these models is the dot-product self-attention mechanism, which learns self-alignment between tokens in an input sequence by estimating the relative importance of each token with respect to all others. The mechanism then transforms each token into a weighted average of the feature representations of the other tokens with weights proportional to the learned importance scores. The relative importance scores capture contextual information among tokens and are key to the success of the transformer architecture (Vig & Belinkov, 2019; Tenney et al., 2019; Cho et al., 2014; Parikh et al., 2016; Lin et al., 2017).

Even though deep transformer-based models have achieved notable success, they are prone to the representation collapse issue, where all token representations become nearly identical as more layers are added. This phenomenon, often referred to as the “over-smoothing” problem, substantially reduces the transformers’ ability to represent diverse features (Shi et al., 2022; Wang et al., 2022; Devlin et al., 2018). To demonstrate this phenomenon, we analyze the average cosine similarity between token pairs across layers in a softmax transformer trained for the Imagenet classification tasks. As shown in Figure 2, the cosine similarity between tokens increases with depth. In the final layers, the cosine similarity scores are just under 0.9, suggesting a high level of similarity among token representations.

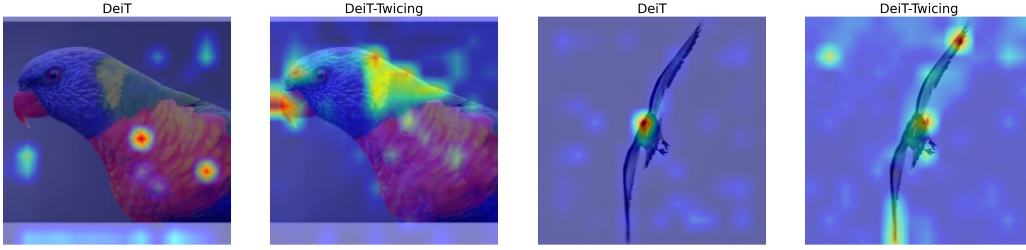


Figure 1: DeiT (Touvron et al., 2021) and DeiT-Twicing (ours) attention heatmaps. Our model shows better representational capacity compared to the baseline by paying attention to more meaningful parts of objects while DeiT attention scores are collapsed to one or few points.

A prior line of research explores representation collapse in transformers through the lens of image denoising, showing that self-attention computation is equivalent to a gradient descent step towards minimizing energy functional that promotes smoothness in the input image (Nguyen et al., 2023; Gilboa & Osher, 2007). Additionally, investigating the over-smoothing phenomenon from a graph-based perspective has gained significant attention in recent studies (Wu et al., 2023; Shi et al., 2022).

Contribution. In this work, we take the connection between the self-attention mechanism and the nonlocal-means image smoothing filter (Buades et al., 2005) further, and show that rapidly vanishing eigenvalues of associated NLM filter across iterations is a major cause of representation collapse in transformers. The NLM similarity matrix, the heart of NLM smoothing procedure, computes pairwise similarities between image patches based on intensity differences, effectively serving as a weight matrix in the smoothing process. We then propose the Twicing Attention, a novel attention mechanism, redesigned from the modified NLM smoothing operation that is tailored to decrease the rate of decay of the eigenvalues of the NLM similarity matrix and thereby offering advantages over the standard NLM based self-attention. In particular, we establish a connection between our modification technique and the twicing kernels in nonparametric regression (Stuetzle & Mittal, 1979; Newey et al., 2004; Abdous, 1995), uncovering the modified NLM filter’s ability to exploit meaningful information in the residuals of each transformer layer after applying a smoothing operation. In summary, our contributions are three-fold:

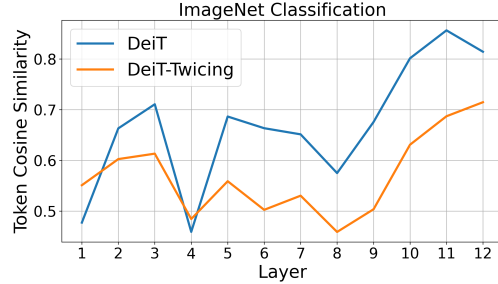


Figure 2: Average token cosine similarities across layers of DeiT and DeiT-Twicing over 100 random samples. Our model retains better token diversity compared to the baseline.

1. We develop the novel Twicing Attention mechanism, a self-attention mechanism variant that promotes better token diversity across transformer layers **which also enjoys enhanced robustness**.
2. We develop a theoretical framework highlighting the effectiveness of Twicing Attention in mitigating representational collapse by decelerating the rate of eigenvalue vanishing phenomenon.
3. We show, through the lens of twicing kernels in nonparametric regression, how unattended but useful residual information between self-attention input and output can be used as a self-correction at each transformer layer.

Moreover, we empirically validate the performance improvements of Twicing Attention over standard self-attention in large-scale tasks such as ImageNet-1K classification (Touvron et al., 2021), ADE20K image segmentation (Strudel et al., 2021) and WikiText-103 language modelling (Merity et al., 2016), and offer additional insights into its implementation with minimal additional computational overhead. We also assess its robustness against adversarial attacks, data contamination, and various distribution shifts.

Organization. The paper is written in the following structure: In Section 2, we introduce the reader with some background context on self-attention mechanism and its connection to image smoothing operation as a warm up to achieve better readability overall. In Section 3, we leverage the connection between self-attention mechanism and nonlocal-means (NLM) smoothing filters to show that representation collapse phenomenon is particularly caused by low-pass behaviour of such filtering procedure. Then, we propose a novel technique to alleviate the low-pass behaviour of associated NLM smoothing, thereby enabling a redesign of the standard self-attention mechanism with better expressive power across the transformer layers. In Section 4, we present our experimental results using Twicing Attention while Section 6 contains a brief overview of related work in the literature. Finally, we end with concluding remarks in Section 7 and defer most of the technical proofs and derivations as well as extra experimental observations to appendix.

2 BACKGROUND

2.1 SELF-ATTENTION MECHANISM

Given an input sequence $\mathbf{X} = [\mathbf{x}_1, \dots, \mathbf{x}_N]^\top \in \mathbb{R}^{N \times D_x}$ of N feature vectors, the self-attention mechanism transforms the input to $\mathbf{U} := [\mathbf{u}_1, \dots, \mathbf{u}_N]^\top \in \mathbb{R}^{N \times D_x}$ as follows:

$$\begin{aligned} \mathbf{u}(i) &= \sum_{j=1}^N \text{softmax} \left(\frac{\mathbf{x}_i^\top \mathbf{W}_K^\top \mathbf{W}_Q \mathbf{x}_j}{\sqrt{D}} \right) \mathbf{W}_V \mathbf{x}_j \\ &= \sum_{j=1}^N \text{softmax} \left(\frac{\mathbf{q}_i^\top \mathbf{k}_j}{\sqrt{D}} \right) \mathbf{v}_j \end{aligned} \quad (1)$$

for $i = 1, \dots, N$, where $\text{softmax}(a_j) := \text{softmax}(\mathbf{a})_j$ for $\mathbf{a} = [a_1, \dots, a_N]$ is an abuse of notation for convenience. The vectors $\mathbf{q}_i, \mathbf{k}_j$, and \mathbf{v}_j , $j = 1, \dots, N$, are the query, key, and value vectors, respectively. They are computed as $\mathbf{Q} := [\mathbf{q}_1, \dots, \mathbf{q}_N]^\top = \mathbf{X} \mathbf{W}_Q^\top \in \mathbb{R}^{N \times D}$, $\mathbf{K} := [\mathbf{k}_1, \dots, \mathbf{k}_N]^\top = \mathbf{X} \mathbf{W}_K^\top \in \mathbb{R}^{N \times D}$, and $\mathbf{V} := [\mathbf{v}_1, \dots, \mathbf{v}_N]^\top = \mathbf{X} \mathbf{W}_V^\top \in \mathbb{R}^{N \times D_v}$, where $\mathbf{W}_Q, \mathbf{W}_K \in \mathbb{R}^{D \times D_x}$, $\mathbf{W}_V \in \mathbb{R}^{D_v \times D_x}$ are the weight matrices. Eqn. 1 can be expressed in matrix form as:

$$\mathbf{U} = \text{softmax} \left(\frac{\mathbf{Q} \mathbf{K}^\top}{\sqrt{D}} \right) \mathbf{V}, \quad (2)$$

where the softmax function is applied row-wise to the matrix $\mathbf{Q} \mathbf{K}^\top / \sqrt{D}$. We refer to transformers built with Eqn. 2 as standard transformers or just transformers.

2.2 NONLOCAL VARIATIONAL DENOISING FRAMEWORK FOR SELF-ATTENTION

Based on the framework established by (Nguyen et al., 2023), we first consider the output matrix $\mathbf{U} := [\mathbf{u}(1), \dots, \mathbf{u}(N)]^\top \in \mathbb{R}^{N \times D}$ in self-attention as given by Eqn. 2 in Section 1.1. Let $\Omega \subset \mathbb{R}, x \in \Omega$, and $\mathbf{u}(x) := [u_1(x), \dots, u_D(x)]^\top$ be a real vector-valued function, $\mathbf{u} : \Omega \rightarrow \mathbb{R}^D, \mathbf{u} \in L^2(\Omega)$. The output matrix \mathbf{U} in self-attention discretizes the function $\mathbf{u}(x)$ with respect to x . In the context of signal/image denoising, \mathbf{U} can be considered as the *desired clean signal*, and $\mathbf{u}(x)$ is its corresponding intensity function denoting the signal values at the position $x \in \Omega$. We further let the observed intensity function $\mathbf{f}(x)$ denote the values of the *observed noisy signal* at $x \in \Omega$, $\mathbf{f} : \Omega \rightarrow \mathbb{R}^D, \mathbf{f} \in L^2(\Omega)$. For example, $\mathbf{f}(x)$ can be given as

$$\mathbf{f}(x) = \mathbf{u}(x) + \mathbf{n}(x), \quad (3)$$

where \mathbf{n} is the additive noise (see Eqn. 1 of (Buades et al., 2005)). We wish to reconstruct $\mathbf{u}(x)$ from $\mathbf{f}(x)$. Following the variational denoising method proposed in (Gilboa & Osher, 2007), the denoised image $\mathbf{u}(x)$ can be obtained by minimizing the following regularized functional with respect to \mathbf{u} :

$$E(\mathbf{u}, \mathbf{f}) = J_w(\mathbf{u}) + G(\mathbf{u}, \mathbf{f}) = \frac{1}{2} \int_{\Omega \times \Omega} \|\mathbf{u}(x) - \mathbf{u}(y)\|_2^2 w(x, y) dx dy + \frac{\lambda}{2} \int_{\Omega} \|\mathbf{u}(x) - \mathbf{f}(x)\|_2^2 dx. \quad (4)$$

Here, $J_w(\mathbf{u}) = \frac{1}{2} \int_{\Omega \times \Omega} \|\mathbf{u}(x) - \mathbf{u}(y)\|_2^2 w(x, y) dx dy$ is a nonlocal functional of weighted differences. The weights $w(x, y)$ represent the affinity between signal values at positions x and y .

For example, for images, $w(x, y)$ captures the proximity between pixels x and y in the image. $J(\mathbf{u})$ works as a regularizer. Minimizing $J(\mathbf{u})$ promotes the smoothness of \mathbf{u} and penalizes high-frequency noise in the signal as discussed in the next section. Adding the convex fidelity term $G(\mathbf{u}, \mathbf{f}) = \frac{\lambda}{2} \int_{\Omega} \|\mathbf{u}(x) - \mathbf{f}(x)\|_2^2 dx$, with the regularization parameter λ , to the functional $J(\mathbf{u})$ allows the denoised signal $\mathbf{u}(x)$ to preserve relevant information in the observed noisy signal $\mathbf{f}(x)$. In the following section, we show that NLM algorithm for image filtering corresponds to a gradient descent step to minimize the functional J_{ω} .

2.3 TRANSFORMERS IMPLEMENT ITERATIVE SMOOTHING

Note that the functional $J_w(\mathbf{u})$ imposes a stronger penalty on discontinuities or sharp transitions in the input signal \mathbf{u} , thereby promoting smoothness throughout the signal. To get the minimizer of $E(\mathbf{u}, \mathbf{f})$, we consider the following system of equation:

$$\frac{\partial E(\mathbf{u}(x), \mathbf{f}(x))}{\partial \mathbf{u}(x)} = \frac{\partial J_w(\mathbf{u}(x))}{\partial \mathbf{u}(x)} + \lambda(\mathbf{u}(x) - \mathbf{f}(x)) = 0, \quad \forall x \in \Omega. \quad (5)$$

Direct gradient calculation, as detailed in Appendix A.3, then yields

$$\int_{\Omega} (\mathbf{u}(x) - \mathbf{u}(y)) w(x, y) dy + \lambda(\mathbf{u}(x) - \mathbf{f}(x)) = 0, \quad \forall x \in \Omega. \quad (6)$$

Rearranging the terms in Eqn. 6, we obtain

$$\mathbf{u}(x) = \frac{\lambda \mathbf{f}(x) + \int_{\Omega} w(x, y) \mathbf{u}(y) dy}{\lambda + \int_{\Omega} w(x, y) dy}, \quad \forall x \in \Omega. \quad (7)$$

It is worth noting that Eqn. 7 becomes NLM filter with weights $w(x, y)$ when $\lambda = 0$ (see Eqn. 2 of (Buades et al., 2005)). In order to establish a connection between NLM and self-attention, let $\mathbf{k}(x) := [k_1(x), \dots, k_D(x)]^\top$ be a real vector-valued function, $\mathbf{k} : \Omega \rightarrow \mathbb{R}^D$, $\mathbf{k} \in L^2(\Omega)$. Similar to $\mathbf{u}(x)$ and $\mathbf{v}(x)$, we can discretize $\mathbf{k}(x)$ on a 1-D grid to attain the key vectors $\mathbf{k}(1), \dots, \mathbf{k}(N) \in \mathbb{R}^D$, which form the key matrix $\mathbf{K} := [\mathbf{k}(1), \dots, \mathbf{k}(N)]^\top \in \mathbb{R}^{N \times D}$ in self-attention as defined in Eqn. 2. Neglecting the symmetry of the kernel, we choose $w(x, y) = \exp(\mathbf{q}(x)^\top \mathbf{k}(y) / \sqrt{D})$ and rewrite Eqn. (7) with $\lambda = 0$ as follows:

$$\mathbf{u}(x) = \frac{\int_{\Omega} \exp(\mathbf{q}(x)^\top \mathbf{k}(y) / \sqrt{D}) \mathbf{u}(y) dy}{\int_{\Omega} \exp(\mathbf{q}(x)^\top \mathbf{k}(y) / \sqrt{D}) dy}, \quad \forall x \in \Omega. \quad (8)$$

In line with the methodology proposed by (Nguyen et al., 2023), the Monte-Carlo discretization of the above expression with respect to $x, y \in \Omega$ yields

$$\mathbf{u}(i) = \frac{\sum_{j=1}^N \exp(\mathbf{q}(i)^\top \mathbf{k}(j) / \sqrt{D}) \mathbf{u}(j)}{\sum_{j=1}^N \exp(\mathbf{q}(i)^\top \mathbf{k}(j) / \sqrt{D})}, \quad (9)$$

for which the following iterative solver is a natural choice:

$$\begin{cases} \mathbf{u}^{\ell+1}(i) &= \frac{\sum_{j=1}^N \exp(\mathbf{q}(i)^\top \mathbf{k}(j) / \sqrt{D}) \mathbf{u}^{\ell}(j)}{\sum_{j=1}^N \exp(\mathbf{q}(i)^\top \mathbf{k}(j) / \sqrt{D})}, \quad \forall \ell \in \mathbb{N}, \\ \mathbf{u}^0(i) &= \mathbf{f}(i), \end{cases}$$

where ℓ is an iteration step. It can be seen that setting $\lambda = 0$ and $\mathbf{u}^{\ell}(j) = \mathbf{v}^{\ell}(j)$, one iteration step becomes

$$\mathbf{u}^{\ell+1}(i) = \frac{\sum_{j=1}^N \exp(\mathbf{q}(i)^\top \mathbf{k}(j) / \sqrt{D}) \mathbf{v}^{\ell}(j)}{\sum_{j=1}^N \exp(\mathbf{q}(i)^\top \mathbf{k}(j) / \sqrt{D})} = \sum_{j=1}^N \text{softmax}\left(\frac{\mathbf{q}(i)^\top \mathbf{k}(j)}{\sqrt{D}}\right) \mathbf{v}^{\ell}(j), \quad (10)$$

which is equivalent to the self-attention computation given by Eqn. (1).

3 HARNESSING UNATTENDED RESIDUAL INFORMATION VIA TWICING ATTENTION

In this section, we shall associate the representation collapse phenomenon with the rapidly vanishing spectrum of NLM similarity matrix during the iterative process, and then propose a method to alleviate this issue. Then, we will give deeper theoretical support for the modification method before proposing our Twicing Attention associated with this modified NLM filter.

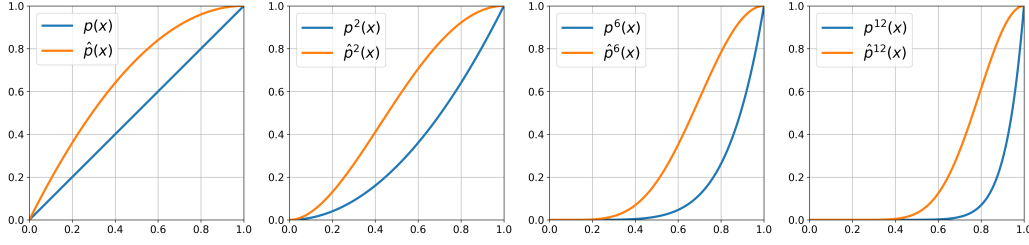


Figure 3: Dynamics of $p^n(x) = x^n$ and $\hat{p}^n(x) = (2x - x^2)^n$ for $n = 1, 2, 6, 12$.

3.1 VANISHING EIGENVALUES IN ITERATIVE NLM FILTERING

The denoising iteration can be written as the matrix-vector multiplication

$$\mathbf{u}^1 = \mathbf{D}^{-1} \mathbf{W} \mathbf{u}^0, \quad (11)$$

where \mathbf{W} is an $N \times N$ matrix given by $\mathbf{W}_{ij} = w(i, j)$, and \mathbf{D} is a diagonal matrix with $\mathbf{D}_{ii} = \sum_{j=1}^N \mathbf{W}_{ij}$. Introducing the averaging operator $\mathbf{A} = \mathbf{D}^{-1} \mathbf{W}$, the denoising iteration Eqn. 11 becomes $\mathbf{u}_d = \mathbf{A} \mathbf{u}$. The matrix \mathbf{A} is conjugate to the positive definite matrix $\mathbf{S} = \mathbf{D}^{-1/2} \mathbf{W} \mathbf{D}^{-1/2}$ via $\mathbf{A} = \mathbf{D}^{-1/2} \mathbf{S} \mathbf{D}^{1/2}$. This implies that \mathbf{A} has a complete set of right eigenvectors $\{\boldsymbol{\xi}_j\}_{j=1}^N$ and positive eigenvalues $1 = \lambda_1 \geq \lambda_2 \geq \dots \geq \lambda_N > 0$. The largest eigenvalue is $\lambda_1 = 1$, corresponding to the trivial all-ones right eigenvector ($\mathbf{A} \mathbf{1} = \mathbf{1}$). We expand the signal vector \mathbf{u} in the eigenbasis as $\mathbf{u} = \sum_{j=1}^N c_j \boldsymbol{\xi}_j$, where $c_j = \langle \boldsymbol{\xi}_j, \mathbf{u} \rangle$. Applying one step of NLM gives

$$\mathbf{A} \mathbf{u} = \sum_{j=1}^N c_j \mathbf{A} \boldsymbol{\xi}_j = \sum_{j=1}^N \lambda_j c_j \boldsymbol{\xi}_j.$$

Iteratively applying NLM n times, however, yields

$$\mathbf{A}^n \mathbf{u} = \sum_{j=1}^N \lambda_j^n c_j \boldsymbol{\xi}_j \quad (12)$$

by the same argument. Eqn. 12 reveals that denoising is accomplished by projecting the image onto the basis $\{\boldsymbol{\xi}_j\}_{j=1}^N$ and attenuating the contributions of the eigenvectors associated with smaller eigenvalues. Observing that in Eqn. 12, the dynamics of eigenvalues are represented as

$$p^n(\mathbf{A}) \mathbf{u} = \sum_{j=1}^N p^n(\lambda_j) c_j \boldsymbol{\xi}_j, \quad (13)$$

where $p(\lambda) = \lambda$, an identity polynomial whose iterations exhibit steep inclines near $\lambda = 1$ and declines sharply towards zero elsewhere. This results in the iterations converging rapidly toward a constant degenerate solution losing salient information in the input.

3.2 LEVERAGING A QUADRATIC KERNEL TOWARDS BETTER INFORMATION CAPACITY

In this section, we revisit the eigenvector expansion of the matrix \mathbf{A} as indicated in Eqn. 12. Although, in theory, high-frequency noise is effectively captured by the eigenvectors corresponding to the smallest eigenvalues, in practice, the iterative denoising process can also suppress the contributions of eigenvectors with larger eigenvalues, leading to potential information loss.

To address this issue, we work out an alternative polynomial dynamics $\hat{p}_n(\cdot)$, which aims to: (*eigenvalue enhancement*) maximally enhance eigenvalues such that $\hat{p}_n(\lambda) \geq p_n(\lambda)$ for all $\lambda \in [0, 1]$, and (*0-1 boundedness*) ensure that values remain within the range $[0, 1]$ to prevent any eigenvalue from exploding limits as $n \rightarrow \infty$, thereby ensuring $-\infty < 0 \leq \lim_{n \rightarrow \infty} \hat{p}_n(\lambda) \leq 1 < \infty$. Owing to the computational overhead associated with higher-degree polynomials, we limit our focus to quadratic polynomials. By setting $\hat{p}(0) = 0$, general form of such polynomials is given by $\hat{p}(\lambda) = a\lambda + b\lambda^2$. Conditions (*eigenvalue enhancement*) and (*0-1 boundedness*) imply $1 \geq \hat{p}(1) \geq p(1) = 1$, leading to $b = 1 - a$. This constraint reformulates \hat{p} as:

$$\hat{p}(\lambda) = a\lambda + (1 - a)\lambda^2. \quad (14)$$

Basic analysis reveals that \hat{p} attains its maximum at $\lambda_a = \frac{a}{2(a-1)}$, which is feasible for all $a \notin (0, 2)$. To satisfy condition (0-1 boundedness), we determine a by solving $\hat{p}(\lambda_a) = 1$, yielding a unique solution of $a = 2$. This confirms that the optimal quadratic polynomial fulfilling both conditions (eigenvalue enhancement) and (0-1 boundedness) is $\hat{p}(\lambda) = 2\lambda - \lambda^2$. Figure 3 illustrates that $\hat{p}^n(\lambda)$ and $p^n(\lambda)$ perform similarly in discarding small eigenvalues near 0, essential for effective noise removal. However, $\hat{p}^n(\lambda)$ remains significantly larger near 1, thus better retaining the salient information captured by the input. This observation suggests using $2\mathbf{A} - \mathbf{A}^2$ as a candidate similarity matrix for smoothing the given input without drastically losing mid-ranged eigenvalues and, thus, being capable of capturing more salient information.

3.3 WHY $2\mathbf{A} - \mathbf{A}^2$ HELPS: THEORETICAL GROUNDING

Now we shall attempt to provide deeper theoretical insights on the benefits of employing $2\mathbf{A} - \mathbf{A}^2$ as a step denoiser, or a similarity matrix in general. First, we demonstrate in Proposition 1 that it achieves substantially slower decay rate of representational capacity in the long run. The connection to twicing kernels, from which the paper title originates, is established and Proposition 2 is presented to demonstrate how these kernels effectively reduce estimation bias in nonparametric regression, another smoothing procedure associated with self-attention.

Mitigating representation collapse. To rigorously analyze the differences in denoising dynamics between the kernels $p(\mathbf{A}) = \mathbf{A}$ and $\hat{p}(\mathbf{A}) = 2\mathbf{A} - \mathbf{A}^2$, we define eigencapacity, which correlates with the model’s information representation capacity, in Definition 1. Then, we demonstrate in Proposition 1 that the eigencapacity of the former kernel decays at a significantly faster rate compared to that of the latter.

Definition 1 (Eigencapacity). *Let $p \in C[0, 1]$ and $p(\mathbf{A})$ represent the filter kernel applied during the n^{th} denoising step, as specified by Eqn. 13. The eigencapacity of this step, denoted by $\kappa_n(p)$, is defined by the integral*

$$\kappa_n(p) := \int_0^1 p^n(x) dx. \quad (15)$$

Note that $\kappa_n(p)$, which represents the area under the curve $p^n(x)$ over the interval $x \in [0, 1]$, exhibits a strong correlation with (the sum of) the well-preserved magnitudes of the eigenvalues of $p^n(\mathbf{A})$ at iteration step n . This correlation arises because the integral of $p^n(x)$ over this range provides an effective approximation of this sum, particularly for matrices of considerable size since mean value theorem for definite integrals implies that

$$\frac{1}{N} \sum_{i=1}^N p^n(\lambda_i) \approx \int_0^1 p^n(x) \rho(x) dx = \rho(c) \kappa_n(p)$$

for some $c \in [0, 1]$, where ρ is a PDF of eigenvalue distribution. This observation underscores the integral’s utility in approximating eigenvalue-related characteristics of the filter dynamics represented by $p^n(\mathbf{A})$. In the following Proposition 1, we show that the eigencapacity of $2\mathbf{A} - 2\mathbf{A}^2$ decays at significantly slower rate than \mathbf{A} .

Proposition 1 (Representational capacity decay rates). *Consider a denoising process employing the filter kernels $p(\mathbf{A}) = \mathbf{A}$ and $\hat{p}(\mathbf{A}) = 2\mathbf{A} - \mathbf{A}^2$. The eigencapacity $\kappa_n(\hat{p})$ decays at a rate of $\mathcal{O}(n^{-1/2})$, in contrast to $\mathcal{O}(n^{-1})$ for $\kappa_n(p)$. Specifically, the behavior of these eigencapacities as $n \rightarrow \infty$ is given by:*

$$\kappa_n(p) \sim \frac{1}{n}, \quad (16)$$

$$\kappa_n(\hat{p}) \sim \frac{\sqrt{\pi}}{2\sqrt{n}}. \quad (17)$$

Remark 1. *Due to the equivalence that has been established between NLM smoothing and self-attention computation in Section 2.3, Proposition 1 demonstrates that if $2\mathbf{A} - \mathbf{A}^2$ was used as a similarity matrix in self-attention mechanism, the output would correspond to a nonlocal smoothing operation for which the convergence to a degenerate solution is significantly slower and, thus, capable of maintaining representational capacity for more iterations.*

We refer the reader to Appendix A.1 for the proof of Proposition 1.

Relation to twicing kernels in nonparametric regression. Equivalence between standard self-attention computation and Nadaraya-Watson estimator using isotropic Gaussian kernels in nonparametric regression has been established and used in numerous recent works (Nguyen et al., 2022; Han et al., 2023; Nielsen et al., 2024). In particular, it has been shown that the output of a self-attention block is a discrete form of convolution of Gaussian kernel with bandwidth \sqrt{D} and the value function (detailed in Appendix A.4). We reinterpret attention computation as $2\mathbf{A} - \mathbf{A}^2$ rather than \mathbf{A} in the nonparametric regression setting. If multiplying by the attention matrix \mathbf{A} is equivalent to using some kernel K for NW estimation, then using \mathbf{A}^2 is equivalent to applying the convolved kernel $K * K$ instead of K (see Appendix A.5).

Therefore, while standard self-attention computation implicitly performs Nadaraya-Watson estimator by employing the kernel K , attention computation with $2\mathbf{A} - \mathbf{A}^2$ is equivalent to employing the modified kernel $2K - K * K$, which is exactly the same as applying the *kernel twicing* procedure to the original regression kernel (Stuetzle & Mittal, 1979; Newey et al., 2004; Abdous, 1995). This constructs higher order kernels with small bias property (SBP) which refers to a kernel’s ability to reduce the leading-order term in the bias of the estimator as demonstrated in Proposition 2 below.

Proposition 2 (Twicing kernels reduce the estimator bias). *Let $K(u)$ be a symmetric kernel function used in the Nadaraya-Watson estimator with bandwidth h . Define a new kernel $\hat{K}(u)$ as*

$$\hat{K}(u) = 2K(u) - (K * K)(u),$$

*where $(K * K)(u)$ denotes the convolution of $K(u)$ with itself. Then, the kernel $\hat{K}(u)$ yields a Nadaraya-Watson estimator with a smaller bias than that using $K(u)$.*

Remark 2. *Due to the relation that has been established between $2\mathbf{A} - \mathbf{A}^2$ and $2K - K * K$, Proposition 2 implies that if $2\mathbf{A} - \mathbf{A}^2$ was used as a similarity matrix in self-attention mechanism, the output would correspond to a Nadaraya-Watson estimator with lower bias and arguably less sensitive to bandwidth selection (Newey et al., 2004). This reduced sensitivity mitigates the bias fluctuations often introduced by slight adjustments, making the attention mechanism inherently more resilient to minor adversarial perturbations and improve model’s robustness in general (Chernozhukov et al., 2022).*

The proof of Proposition 2 is provided in Appendix A.2. For a comprehensive statistical discussion on the topic, we direct the reader to (Newey et al., 2004) and the references therein.

Twicing kernels benefit from residuals. Recall that we have established connection between self-attention matrices \mathbf{A} and $2\mathbf{A} - \mathbf{A}^2$ to regression kernels K and $2K - K * K$, respectively. Therefore, we use smoothing and computing the attention output interchangeably. Now we provide a core constructive difference between the two kernel computations. Given a kernel-type smoother \mathbf{A} and observations $\mathbf{V}^\ell(x)$ at iteration ℓ , twicing procedure takes the following three steps:

1. Smooth $\mathbf{V}^\ell(x)$ and obtain $\mathbf{A}\mathbf{V}^\ell(x)$.
2. Smooth the residual $\mathbf{V}^\ell(x) - \mathbf{A}\mathbf{V}^\ell(x)$ and obtain the correction $\mathbf{A}(\mathbf{V}^\ell(x) - \mathbf{A}\mathbf{V}^\ell(x)) = (\mathbf{A} - \mathbf{A}^2)\mathbf{V}^\ell(x)$.
3. Combine Step 1 and Step 2 and define $(2\mathbf{A} - \mathbf{A}^2)\mathbf{V}^\ell(x)$ as the new estimator.

Note that the final estimator actually consists of two terms: the first term corresponds to the denoised image via the filter \mathbf{A} , and the second term is the residual $\mathbf{V}^\ell - \mathbf{A}\mathbf{V}^\ell$, which is also smoothed with \mathbf{A} . Therefore, denoising with kernel $\hat{p}(\mathbf{A})$ is equivalent to denoising with kernel $p(\mathbf{A})$ and subsequently feeding the smoothed method noise of this denoising step back into the output of the current iteration to effectively extracts salient information remaining in the residual and reincorporates it into the denoising output.

3.4 TWICING ATTENTION: FULL TECHNICAL FORMULATION

Stemming from the theoretical benefits discussed in the previous sections, we formulate Twicing Attention as follows:

Definition 2 (Twicing Attention). *Given query $\mathbf{Q}^\ell = [\mathbf{q}_1^\ell, \dots, \mathbf{q}_N^\ell]^\top \in \mathbb{R}^{N \times D}$, key $\mathbf{K}^\ell = [\mathbf{k}_1^\ell, \dots, \mathbf{k}_N^\ell]^\top \in \mathbb{R}^{N \times D}$, and value $\mathbf{V}^\ell = [\mathbf{v}_1^\ell, \dots, \mathbf{v}_N^\ell]^\top \in \mathbb{R}^{N \times D}$ matrices as in Section 2.1 at*

Table 1: Top-1 and Top-5 Test Accuracy on ImageNet corrupted by projected gradient descent (PGD), fast gradient sign method (FGSM), and simultaneous perturbation stochastic approximation (SPSA).

Model	ImageNet		PGD		FGSM		SPSA	
	Top 1	Top 5	Top 1	Top 5	Top 1	Top 5	Top 1	Top 5
<i>DeiT</i> (Touvron et al., 2021)	72.00	91.14	8.16	22.37	29.88	63.26	66.41	90.29
<i>NeuTRENO</i> (Nguyen et al., 2023)	72.44	91.39	8.85	23.83	31.43	65.96	66.98	90.48
DeiT-Twicing [10-12]	72.31	91.24	8.66	22.58	31.63	64.74	66.47	90.49
DeiT-Twicing	72.60	<u>91.33</u>	9.15	24.10	32.28	<u>65.67</u>	67.12	90.53
<i>FAN</i> (Zhou et al., 2022)	77.09	93.72	11.91	24.11	33.81	65.25	67.15	92.14
FAN-Twicing	77.18	94.02	12.80	28.86	35.52	67.23	68.89	93.75

Table 2: Evaluation of the performance of DeiT and DeiT-Twicing in ImageNet classification under the presence of different corruptions, using appropriate evaluation metrics for each.

Dataset Metric	ImageNet-R Top 1	ImageNet-A Top 1	ImageNet-C mCE (\downarrow)	ImageNet-C (Extra) mCE (\downarrow)
<i>DeiT</i> (Touvron et al., 2021)	32.22	6.97	72.21	63.68
DeiT-Twicing [10-12]	<u>32.31</u>	8.14	70.25	<u>62.63</u>
DeiT-Twicing	32.74	<u>7.66</u>	<u>70.33</u>	62.46
<i>FAN</i> (Zhou et al., 2022)	42.24	12.33	60.71	52.70
FAN-Twicing	42.36	<u>12.30</u>	60.48	52.21

ℓ^{th} layer of transformer, the output of Twicing Attention mechanism is computed as:

$$\mathbf{U}^\ell = (2\mathbf{A} - \mathbf{A}^2)\mathbf{V}^\ell, \quad (18)$$

where $\mathbf{A} := \text{softmax}(\mathbf{Q}^\ell \mathbf{K}^{\ell\top} / \sqrt{D})$ and the softmax function is applied row-wise.

Remark 3. Even though Definition 2 gives Twicing Attention computation as in Eqn. 18, we use the following equivalent, a twicing procedure-inspired form in practice:

$$\mathbf{U}^\ell = \mathbf{A}\mathbf{V}^\ell + \mathbf{A}(\mathbf{V}^\ell - \mathbf{A}\mathbf{V}^\ell). \quad (19)$$

In other words, instead of computing the square of attention matrix \mathbf{A}^2 , we decompose Eqn. 18 into regular self-attention output and smoothed residual parts as $\mathbf{A}\mathbf{V}^\ell + \mathbf{A}(\mathbf{V}^\ell - \mathbf{A}\mathbf{V}^\ell)$. This allows us to compute $\mathbf{A}\mathbf{V}^\ell$ once and reuse it in the residual to replace attention squaring operation, which is $\mathcal{O}(N^3)$, with cheaper matrix multiplication of $\mathcal{O}(N^2D)$ runtime complexity matching the standard self-attention computation.

Algorithm 1 presents a pseudocode for implementing Twicing Attention as given by Eqn. 18 on top of conventional self-attention. Notice that in Algorithm 1, instead of computing the square of attention matrix \mathbf{A}^2 , we decompose Eqn. 18 into regular self-attention output and smoothed residual parts as discussed and Remark 3.

Algorithm 1 Computation of Twicing Attention

```

1: function TWICING_ATTENTION( $\mathbf{Q}, \mathbf{K}, \mathbf{V}, D$ )
2:    $\mathbf{A} \leftarrow \text{SOFTMAX}(\mathbf{Q} \times \mathbf{K}^\top \times \frac{1}{\sqrt{D}})$ 
3:    $\text{SmoothV} \leftarrow \mathbf{A} \times \mathbf{V}$ 
4:    $\text{Res} \leftarrow \mathbf{V} - \text{SmoothV}$ 
5:   return  $\text{SmoothV} + \mathbf{A} \times \text{Res}$ 
6: end function
```

4 EXPERIMENTAL RESULTS

In this section, we empirically justify the advantage of Twicing Attention over baseline transformers with standard self-attention mechanism. Whenever we employ our Twicing Attention to replace the standard one in a given model, we append a *Twicing* suffix to imply this in the reports. Moreover, if Twicing Attention is inserted in specific transformer layers only, we specify the layer indices in square brackets ([10-12] for Twicing Attention in layers 10, 11 and 12, etc.). We evaluate our method on Wikitext-103 modeling both under clean and Word Swap contamination (Merity et al., 2016), and ImageNet-1K classification under a wide range of attacks (Deng et al., 2009; Russakovsky et al., 2015) as described in details in the following paragraphs.

Table 3: Image segmentation on ADE20K.

Model	Pix. Acc.	Mean Acc.	Mean IoU
<i>DeiT</i>	77.25	44.48	34.73
DeiT-Twicing	77.51	45.53	35.12

Table 4: Test PPL on WikiText-103.

Model	Test PPL	Attacked PPL
<i>Transformer</i>	37.51	55.17
Tr.-Twicing	36.69	54.46

4.1 IMAGE CLASSIFICATION AND SEGMENTATION

Object classification on ImageNet-1K. To demonstrate the advantage of our model, we compare it with the *DeiT* baseline (Touvron et al., 2021) and NeuTRENO (Nguyen et al., 2023) on the ImageNet1K image classification task (Deng et al., 2009). Our model surpasses the *DeiT* baseline, as shown in Table 1 in the clean data setting as well as under adversarial attacks such as fast gradient sign method (FGSM) (Goodfellow et al., 2014), projected gradient descent (PGD) (Madry et al., 2017) with perturbation budget 4/255 and provide a comparison of results for different values of perturbations in appendix, and simultaneous perturbation stochastic approximation (SPSA) (Uesato et al., 2018) with perturbation budget 1/255. Furthermore, Table 2 shows DeiT-Twicing to be consistently more robust than the *DeiT* baseline across various testing conditions, including adversarial examples and out-of-distribution datasets. This includes its performance on the Imagenet-C dataset, which involves common data corruptions and perturbations such as noise addition and image blurring, as well as on Imagenet-A and Imagenet-R datasets, which assess adversarial example handling and out-of-distribution generalization, respectively (Hendrycks et al., 2021). ImageNet-C (Extra) contains four extra image corruption types. They are spatter, gaussian blur, saturate and speckle noise.

When combining with a state-of-the-art robust transformer backbone, *Fully Attentional Network* (FAN) (Zhou et al., 2022), Twicing Attention is able to improve performance in terms of clean accuracy as well as its robustness against adversarial attacks such as PGD and FGSM (with perturbation budget 4/255) as well as SPSA (with perturbation budget 1/255) substantially as included in Table 1. We also find better out-of-distribution generalization in FAN-Twicing over standard FAN except for ImageNet-A benchmark where FAN-Twicing is still highly competitive (see Table 2).

Image Segmentation on ADE20K. On top of the classification task, we compare the performance of the Segmenter models using *DeiT* and *DeiT-Twicing* backbones on the ADE20K (Zhou et al., 2019) image segmentation task to further validate the advantages of our proposed method by adopting the experimental setup of (Strudel et al., 2021). In Table 3, we report the key metrics: pixel accuracy, mean accuracy, and mean intersection over union (IOU). We observe performance boost across all 3 metrics with *DeiT-Twicing* over the *DeiT* baseline (Touvron et al., 2021).

4.2 LANGUAGE MODELING ON WIKITEXT-103

In addition to computer vision tasks, we also evaluate the effectiveness of our model on a large-scale natural language processing application, specifically language modeling on WikiText-103 (Merity et al., 2016). Our language model demonstrates better performance in terms of both test perplexity (PPL) and valid perplexity when compared to the standard *transformer* language model (Vaswani et al., 2017) as shown in Table 4. We also show that test PPL on WikiText-103 contaminated by Word Swap Attack, where words are randomly swapped with a generic token 'AAA'. We follow the setup of (Han et al., 2024) and assess models by training them on clean data before attacking only the test data using an attack rate of 4%.

5 EMPIRICAL ANALYSIS

Representation collapse analysis. We empirically demonstrate in Figure 2 that Twicing Attention mechanism promotes better token diversity and, therefore, it is able to slow down representation collapse phenomenon in transformers. We observe that, in *DeiT*, the average cosine similarity score between tokens quickly exceeds three-quarters, whereas in our model, it remains consistently below this threshold. Additionally, we demonstrate in Figure 1 that our model is indeed capable of retaining better expressive power by being able to pay attention to notably more and important parts of objects in images while *DeiT* indicates collapsed behaviour. See Appendix D.2 for a dozen of additional attention heatmaps supporting the comparative argument.

Table 5: Efficiency comparison between DeiT and DeiT-Twicing models.

Model	Avg. Compute Speed (ms/it)	GFLOPs / sample	Param. Count (M)
<i>DeiT</i> (Touvron et al., 2021)	8.58	1.25	5.7
DeiT-Twicing	9.14	1.33	5.7
DeiT-Twicing [10-12]	8.72	1.27	5.7

Efficiency analysis. As stated in Remark 3, our Twicing Attention mechanism can be implemented with $\mathcal{O}(N^2D)$ runtime complexity, which is on par with the standard self-attention mechanism. Table 5 compares the prediction average compute speed per iteration over 1000 runs as well as the floating-point operations (FLOPs) per sample, which is a measure of trade-off between efficiency (lower FLOPs) and accuracy (higher FLOPs) of models. We observe that employing Twicing Attention only in last 3 layers, the model can still enjoy performance gains over the baseline while seeing almost negligible increase in average compute speed and FLOPs per sample.

6 RELATED WORK

Theoretical Frameworks for Attention. Attention mechanisms have been studied from a range of perspectives. (Tsai et al., 2019) show that attention can be derived from kernel similarity functions and (Tao et al., 2023) explain attention through nonlinear singular value decomposition of asymmetric kernels. Attention has also been explained through ordinary/partial differential equations, Gaussian mixture models, and graph-structured learning (Lu et al., 2019; Sander et al., 2022; Tang & Matteson, 2021; Gabbur et al., 2021; Kreuzer et al., 2021; Zhang & Feng, 2021) or an energy functional minimization associated with a variational image denoising framework (Nguyen et al., 2023). (Nguyen et al., 2022; Han et al., 2024; Nielsen et al., 2024) show that self-attention performs Nadaraya-Watson regression with Gaussian isotropic kernels.

Representation Collapse in Transformers. Representation collapse or over-smoothing in deep transformers has been noted across different domains and applications, including natural language processing (Shi et al., 2022) and computer vision (Wang et al., 2022). In (Shi et al., 2022), the issue is examined within BERT (Devlin et al., 2018), a deep language model, through a graph-based perspective. The study employs hierarchical fusion techniques by retaining the self-attention output across all layers, though this approach is memory-intensive. (Dong et al., 2021) is among the initial efforts towards understanding oversmoothing in transformers through the lens of rank collapse. (Caron et al., 2021) studies the feature maps of self-supervised Vision Transformers (ViTs), uncovering explicit information contained in them about the semantic segmentation of an image, while (Darcet et al., 2024) identifies high-norm token artifacts in these feature maps, arising in low-informative background areas during inference, and proposes a solution using additional register tokens to address this issue.

Robust Transformers. For transformers, robust strategies include an ensemble defense against adversarial attacks Mahmood et al. (2021), position-aware attention scaling with patch-wise augmentation Mao et al. (2022), and a fully-attentional network for state-of-the-art performance on corrupted images Zhou et al. (2022). Efficiency usually refers to optimal performance under ideal conditions, while robustness describes maintaining strong performance under less-than-ideal circumstances. A common trend among robust models, such as (Mao et al., 2022; Han et al., 2023; Zhou et al., 2022), is their reliance on additional computational overhead, often matching or even exceeding that of our proposed model.

7 CONCLUDING REMARKS

In this paper, we introduced the Twicing Attention mechanism, enhancing the transformer’s representational capacity by utilizing residuals between self-attention inputs and outputs. This novel self-attention variant improves token diversity and mitigates representational collapse by leveraging useful residual information as a form of self-correction. We empirically demonstrated performance gains on ImageNet-1k, ADE20K, WikiText-103, and robustness benchmarks with minimal computational overhead by trying selective layer placement for Twicing Attention. However, limitations include its efficient application across transformer all layers with no or negligible additional computation. Ongoing work explores approximation techniques and sparsity to improve efficiency, while extending the theoretical framework to even more practical scenarios remains an open challenge.

Reproducibility Statement. We have made efforts to ensure the reproducibility of our work through several measures. Source codes for our experiments are provided in the supplementary materials of the paper. The details of our experimental settings and computational infrastructure are given in Section 4 and the Appendix. All datasets that we used in the paper are published, and they are easy to find in the Internet. These resources and explanations should allow others to replicate our results with relative ease.

Ethics Statement. Given the nature of our work and contributions, we do not foresee any negative societal and ethical impacts of our work.

REFERENCES

- Belaid Abdous. Computationally efficient classes of higher-order kernel functions. *The Canadian Journal of Statistics / La Revue Canadienne de Statistique*, 23(1):21–27, 1995. doi: 10.2307/3315548.
- Rami Al-Rfou, Dokook Choe, Noah Constant, Mandy Guo, and Llion Jones. Character-level language modeling with deeper self-attention. In *Proceedings of the AAAI conference on artificial intelligence*, volume 33, pp. 3159–3166, 2019.
- Alexei Baevski and Michael Auli. Adaptive input representations for neural language modeling. *arXiv preprint arXiv:1809.10853*, 2018.
- A. Buades, B. Coll, and J.-M. Morel. A non-local algorithm for image denoising. In *2005 IEEE Computer Society Conference on Computer Vision and Pattern Recognition (CVPR’05)*, volume 2, pp. 60–65 vol. 2, 2005. doi: 10.1109/CVPR.2005.38.
- Mathilde Caron, Hugo Touvron, Ishan Misra, Herv’e J’egou, Julien Mairal, Piotr Bojanowski, and Armand Joulin. Emerging properties in self-supervised vision transformers. *2021 IEEE/CVF International Conference on Computer Vision (ICCV)*, pp. 9630–9640, 2021.
- Lili Chen, Kevin Lu, Aravind Rajeswaran, Kimin Lee, Aditya Grover, Misha Laskin, Pieter Abbeel, Aravind Srinivas, and Igor Mordatch. Decision transformer: Reinforcement learning via sequence modeling. *Advances in neural information processing systems*, 34:15084–15097, 2021.
- Victor Chernozhukov, Juan Carlos Escanciano, Hidehiko Ichimura, Whitney K. Newey, and James M. Robins. Locally robust semiparametric estimation. *Econometrica*, 90(4):1501–1535, July 2022. doi: 10.3982/ECTA16294. URL <https://doi.org/10.3982/ECTA16294>.
- Kyunghyun Cho, Bart Van Merriënboer, Caglar Gulcehre, Dzmitry Bahdanau, Fethi Bougares, Holger Schwenk, and Yoshua Bengio. Learning phrase representations using rnn encoder-decoder for statistical machine translation. *arXiv preprint arXiv:1406.1078*, 2014.
- Zihang Dai, Zhilin Yang, Yiming Yang, Jaime Carbonell, Quoc V Le, and Ruslan Salakhutdinov. Transformer-xl: Attentive language models beyond a fixed-length context. *arXiv preprint arXiv:1901.02860*, 2019.
- Timothée Darcet, Maxime Oquab, Julien Mairal, and Piotr Bojanowski. Vision transformers need registers. In *The Twelfth International Conference on Learning Representations*, 2024. URL <https://openreview.net/forum?id=2dn03LLiJ1>.
- Mostafa Dehghani, Stephan Gouws, Oriol Vinyals, Jakob Uszkoreit, and Łukasz Kaiser. Universal transformers. *arXiv preprint arXiv:1807.03819*, 2018.
- Jia Deng, Wei Dong, Richard Socher, Li-Jia Li, Kai Li, and Li Fei-Fei. Imagenet: A large-scale hierarchical image database. In *2009 IEEE conference on computer vision and pattern recognition*, pp. 248–255. Ieee, 2009.
- Jacob Devlin, Ming-Wei Chang, Kenton Lee, and Kristina Toutanova. Bert: Pre-training of deep bidirectional transformers for language understanding. *arXiv preprint arXiv:1810.04805*, 2018.

- Yihe Dong, Jean-Baptiste Cordonnier, and Andreas Loukas. Attention is not all you need: pure attention loses rank doubly exponentially with depth. In Marina Meila and Tong Zhang (eds.), *Proceedings of the 38th International Conference on Machine Learning*, volume 139 of *Proceedings of Machine Learning Research*, pp. 2793–2803. PMLR, 18–24 Jul 2021. URL <https://proceedings.mlr.press/v139/dong21a.html>.
- Prasad Gabbur, Manjot Bilkhu, and Javier Movellan. Probabilistic attention for interactive segmentation. *Advances in Neural Information Processing Systems*, 34:4448–4460, 2021.
- Guy Gilboa and Stanley Osher. Nonlocal linear image regularization and supervised segmentation. *Multiscale Modeling & Simulation*, 6(2):595–630, 2007. doi: 10.1137/060669358.
- Ian J Goodfellow, Jonathon Shlens, and Christian Szegedy. Explaining and harnessing adversarial examples. *arXiv preprint arXiv:1412.6572*, 2014.
- Xing Han, Tongzheng Ren, Tan Minh Nguyen, Khai Nguyen, Joydeep Ghosh, and Nhat Ho. Designing robust transformers using robust kernel density estimation. In *Thirty-seventh Conference on Neural Information Processing Systems*, 2023. URL <https://openreview.net/forum?id=BqTv1Mtuhu>.
- Xing Han, Tongzheng Ren, Tan Nguyen, Khai Nguyen, Joydeep Ghosh, and Nhat Ho. Designing robust transformers using robust kernel density estimation. *Advances in Neural Information Processing Systems*, 36, 2024.
- Dan Hendrycks, Kevin Zhao, Steven Basart, Jacob Steinhardt, and Dawn Song. Natural adversarial examples. In *Proceedings of the IEEE/CVF conference on computer vision and pattern recognition*, pp. 15262–15271, 2021.
- Michael Janner, Qiyang Li, and Sergey Levine. Offline reinforcement learning as one big sequence modeling problem. *Advances in neural information processing systems*, 34:1273–1286, 2021.
- Salman Khan, Muzammal Naseer, Munawar Hayat, Syed Waqas Zamir, Fahad Shahbaz Khan, and Mubarak Shah. Transformers in vision: A survey. *ACM computing surveys (CSUR)*, 54(10s): 1–41, 2022.
- Devin Kreuzer, Dominique Beaini, Will Hamilton, Vincent Létourneau, and Prudencio Tossou. Rethinking graph transformers with spectral attention. *Advances in Neural Information Processing Systems*, 34:21618–21629, 2021.
- Tianyang Lin, Yuxin Wang, Xiangyang Liu, and Xipeng Qiu. A survey of transformers. *AI open*, 3: 111–132, 2022.
- Zhouhan Lin, Minwei Feng, Cicero Nogueira dos Santos, Mo Yu, Bing Xiang, Bowen Zhou, and Yoshua Bengio. A structured self-attentive sentence embedding. *arXiv preprint arXiv:1703.03130*, 2017.
- Ze Liu, Yutong Lin, Yue Cao, Han Hu, Yixuan Wei, Zheng Zhang, Stephen Lin, and Baining Guo. Swin transformer: Hierarchical vision transformer using shifted windows. In *Proceedings of the IEEE/CVF international conference on computer vision*, pp. 10012–10022, 2021.
- Yiping Lu, Zhuohan Li, Di He, Zhiqing Sun, Bin Dong, Tao Qin, Liwei Wang, and Tie-Yan Liu. Understanding and improving transformer from a multi-particle dynamic system point of view. *arXiv preprint arXiv:1906.02762*, 2019.
- Aleksander Madry, Aleksandar Makelov, Ludwig Schmidt, Dimitris Tsipras, and Adrian Vladu. Towards deep learning models resistant to adversarial attacks. *arXiv preprint arXiv:1706.06083*, 2017.
- Kaleel Mahmood, Rigel Mahmood, and Marten Van Dijk. On the robustness of vision transformers to adversarial examples. In *Proceedings of the IEEE/CVF international conference on computer vision*, pp. 7838–7847, 2021.

- Xiaofeng Mao, Gege Qi, Yuefeng Chen, Xiaodan Li, Ranjie Duan, Shaokai Ye, Yuan He, and Hui Xue. Towards robust vision transformer. In *Proceedings of the IEEE/CVF conference on Computer Vision and Pattern Recognition*, pp. 12042–12051, 2022.
- Stephen Merity, Caiming Xiong, James Bradbury, and Richard Socher. Pointer sentinel mixture models. *arXiv preprint arXiv:1609.07843*, 2016.
- Whitney K. Newey, Fushing Hsieh, and James M. Robins. Twicing kernels and a small bias property of semiparametric estimators. *Econometrica*, 72(3):947–962, 2004. ISSN 00129682, 14680262. URL <http://www.jstor.org/stable/3598841>.
- Tam Minh Nguyen, Tan Minh Nguyen, and Richard Baraniuk. Mitigating over-smoothing in transformers via regularized nonlocal functionals. In *Thirty-seventh Conference on Neural Information Processing Systems*, 2023. URL <https://openreview.net/forum?id=3fd776zKmo>.
- Tan Nguyen, Minh Pham, Tam Nguyen, Khai Nguyen, Stanley Osher, and Nhat Ho. Fourierformer: Transformer meets generalized fourier integral theorem. *Advances in Neural Information Processing Systems*, 35:29319–29335, 2022.
- Stefan K. Nielsen, Laziz U. Abdullaev, Rachel Teo, and Tan M. Nguyen. Elliptical attention. *arXiv preprint arXiv:2406.13770*, 2024.
- Ankur P Parikh, Oscar Täckström, Dipanjan Das, and Jakob Uszkoreit. A decomposable attention model for natural language inference. *arXiv preprint arXiv:1606.01933*, 2016.
- Alec Radford, Karthik Narasimhan, Tim Salimans, Ilya Sutskever, et al. Improving language understanding by generative pre-training. 2018.
- Alec Radford, Jeffrey Wu, Rewon Child, David Luan, Dario Amodei, Ilya Sutskever, et al. Language models are unsupervised multitask learners. *OpenAI blog*, 1(8):9, 2019.
- Alec Radford, Jong Wook Kim, Chris Hallacy, Aditya Ramesh, Gabriel Goh, Sandhini Agarwal, Girish Sastry, Amanda Askell, Pamela Mishkin, Jack Clark, et al. Learning transferable visual models from natural language supervision. In *International conference on machine learning*, pp. 8748–8763. PMLR, 2021.
- Colin Raffel, Noam Shazeer, Adam Roberts, Katherine Lee, Sharan Narang, Michael Matena, Yanqi Zhou, Wei Li, and Peter J Liu. Exploring the limits of transfer learning with a unified text-to-text transformer. *Journal of machine learning research*, 21(140):1–67, 2020.
- Olga Russakovsky, Jia Deng, Hao Su, Jonathan Krause, Sanjeev Satheesh, Sean Ma, Zhiheng Huang, Andrej Karpathy, Aditya Khosla, Michael Bernstein, et al. Imagenet large scale visual recognition challenge. *International journal of computer vision*, 115:211–252, 2015.
- Michael E Sander, Pierre Ablin, Mathieu Blondel, and Gabriel Peyré. Sinkformers: Transformers with doubly stochastic attention. In *International Conference on Artificial Intelligence and Statistics*, pp. 3515–3530. PMLR, 2022.
- Han Shi, JIAHUI GAO, Hang Xu, Xiaodan Liang, Zhenguo Li, Lingpeng Kong, Stephen M. S. Lee, and James Kwok. Revisiting over-smoothing in BERT from the perspective of graph. In *International Conference on Learning Representations*, 2022. URL <https://openreview.net/forum?id=dUV91uaXm3>.
- Robin Strudel, Ricardo Garcia, Ivan Laptev, and Cordelia Schmid. Segmenter: Transformer for semantic segmentation. In *Proceedings of the IEEE/CVF international conference on computer vision*, pp. 7262–7272, 2021.
- W. Stuetzle and Y. Mittal. Some comments on the asymptotic behavior of robust smoothers. In T. Gasser and M. Rosenblatt (eds.), *Smoothing Techniques for Curve Estimation*, volume 757 of *Lecture Notes*, pp. 191–195. Springer-Verlag, New York, 1979.
- Binh Tang and David S Matteson. Probabilistic transformer for time series analysis. *Advances in Neural Information Processing Systems*, 34:23592–23608, 2021.

- Qinghua Tao, Francesco Tonin, Panagiotis Patrinos, and Johan AK Suykens. Nonlinear svd with asymmetric kernels: feature learning and asymmetric nyström method. *arXiv preprint arXiv:2306.07040*, 2023.
- Yi Tay, Mostafa Dehghani, Dara Bahri, and Donald Metzler. Efficient transformers: A survey. *ACM Computing Surveys*, 55(6):1–28, 2022.
- Ian Tenney, Dipanjan Das, and Ellie Pavlick. Bert rediscovers the classical nlp pipeline. *arXiv preprint arXiv:1905.05950*, 2019.
- Hugo Touvron, Matthieu Cord, Matthijs Douze, Francisco Massa, Alexandre Sablayrolles, and Hervé Jégou. Training data-efficient image transformers & distillation through attention. In *International conference on machine learning*, pp. 10347–10357. PMLR, 2021.
- Yao-Hung Hubert Tsai, Shaojie Bai, Makoto Yamada, Louis-Philippe Morency, and Ruslan Salakhutdinov. Transformer dissection: a unified understanding of transformer’s attention via the lens of kernel. *arXiv preprint arXiv:1908.11775*, 2019.
- Jonathan Uesato, Brendan O’donoghue, Pushmeet Kohli, and Aaron Oord. Adversarial risk and the dangers of evaluating against weak attacks. In *International Conference on Machine Learning*, pp. 5025–5034. PMLR, 2018.
- Ashish Vaswani, Noam Shazeer, Niki Parmar, Jakob Uszkoreit, Llion Jones, Aidan N Gomez, Łukasz Kaiser, and Illia Polosukhin. Attention is all you need. *Advances in neural information processing systems*, 30, 2017.
- Jesse Vig and Yonatan Belinkov. Analyzing the structure of attention in a transformer language model. *arXiv preprint arXiv:1906.04284*, 2019.
- M. P. Wand and M. C. Jones. *Kernel Smoothing*. CRC Press, Chapman and Hall, 1995.
- Peihao Wang, Wenqing Zheng, Tianlong Chen, and Zhangyang Wang. Anti-oversmoothing in deep vision transformers via the fourier domain analysis: From theory to practice. In *International Conference on Learning Representations*, 2022. URL <https://openreview.net/forum?id=O476oWmiNNp>.
- Xinyi Wu, Amir Ajorlou, Zihui Wu, and Ali Jadbabaie. Demystifying oversmoothing in attention-based graph neural networks. In *Thirty-seventh Conference on Neural Information Processing Systems*, 2023. URL <https://openreview.net/forum?id=Kg65qieiuB>.
- Shaolei Zhang and Yang Feng. Modeling concentrated cross-attention for neural machine translation with gaussian mixture model. *arXiv preprint arXiv:2109.05244*, 2021.
- Bolei Zhou, Hang Zhao, Xavier Puig, Tete Xiao, Sanja Fidler, Adela Barriuso, and Antonio Torralba. Semantic understanding of scenes through the ade20k dataset. *International Journal of Computer Vision*, 127:302–321, 2019.
- Daquan Zhou, Zhiding Yu, Enze Xie, Chaowei Xiao, Animashree Anandkumar, Jiashi Feng, and Jose M Alvarez. Understanding the robustness in vision transformers. In *International Conference on Machine Learning*, pp. 27378–27394. PMLR, 2022.

Supplement to “Transformer Meets Twicing: Harnessing Unattended Residual Information”

Table of Contents

A	Technical Proofs and Derivations	15
A.1	Proof of Proposition 1	15
A.2	Proof of Proposition 2	16
A.3	Derivation of Gradient of J_ω	17
A.4	Equivalence of Self-attention and Nadaraya-Watson Estimator	18
A.5	Equivalence between Self-convolution and Square of Attention Matrix	19
B	Experimental Details and Additional Results	20
B.1	Wikitext-103 Language Modelling and Word Swap Attack	20
B.2	ImageNet Image Classification and Adversarial Attack	20
B.3	Out-of-Distribution Robustness and Data Corruption on ImageNet-A,R,C	21
B.4	ADE20K Image Segmentation	21
C	Compute Resources	21
D	Additional Empirical Analysis	22
D.1	Training Analysis	22
D.2	Extra Attention Heatmap Analysis	22
E	Ablation Studies	22

A TECHNICAL PROOFS AND DERIVATIONS

A.1 PROOF OF PROPOSITION 1

The equivalence in Eqn. 16 is straightforward to obtain since $\kappa_n(p)$ can be calculated as

$$\kappa_n(p) = \int_0^1 p^n(x) dx = \int_0^1 x^n dx = \frac{1}{n+1} \sim \frac{1}{n}.$$

To prove the equivalence given by Eqn. 17, we first observe that

$$\kappa_n(\hat{p}) = \int_0^1 \hat{p}^n(x) dx = \int_0^1 (2x - x^2)^n dx = \frac{1}{2} \int_0^2 (2x - x^2)^n dx,$$

where the last equality is due to the symmetry of $2x - x^2 = 1 - (1 - x)^2$ along $x = 1$. Now, employing a variable change $x = 2y$ yields

$$\begin{aligned} \kappa_n(\hat{p}) &= \frac{1}{2} \int_0^2 (2x - x^2)^n dx = \int_0^1 (4y - 4y^2)^n dy \\ &= 4^n \int_0^1 y^n (1 - y)^n dy = 4^n B(n+1, n+1) \end{aligned} \quad (20)$$

$$= \frac{4^n \Gamma(n+1)^2}{\Gamma(2n+2)} = \frac{4^n (n!)^2}{(2n+1)!}, \quad (21)$$

where $B(x, y)$ and $\Gamma(x)$ denote the Euler Beta function and Gamma function, respectively, and we used the identity $B(x, y) = \Gamma(x)\Gamma(y)/\Gamma(x+y)$ to transform Eqn. 20 into Eqn.21. Now using

Stirling's approximation $n! \sim \sqrt{2\pi n}(n/e)^n$ as $n \rightarrow \infty$ for Eqn. 21, we obtain

$$\begin{aligned}\kappa_n(\hat{p}) &\sim \frac{4^n \cdot 2\pi n^{2n+1}/e^{2n}}{\sqrt{2\pi(2n+1)}(2n+1)^{2n+1}/e^{2n+1}} \\ &= e\sqrt{\frac{\pi}{2}} \frac{1}{\sqrt{2n+1}} \left(\frac{2n}{2n+1}\right)^{2n+1} \\ &= \frac{e\sqrt{\pi}}{2} \frac{1}{\sqrt{n+1/2}} \left(1 - \frac{1}{2n+1}\right)^{2n+1} \\ &\sim \frac{\sqrt{\pi}}{2\sqrt{n}},\end{aligned}\tag{22}$$

where we used the fact that $e^{-1} = \lim_{n \rightarrow \infty} \left(1 - \frac{1}{2n+1}\right)^{2n+1}$ to derive Eqn. 22. \square

A.2 PROOF OF PROPOSITION 2

Proof of Proposition 2. To compare the biases of the estimators using kernels $K(u)$ and $\hat{K}(u)$, we analyze the moments of these kernels, as they determine the bias in kernel estimators.

We begin with showing that \hat{K} has valid kernel properties.

Normalization. Since $K(u)$ is a valid kernel, we have:

$$\int_{-\infty}^{\infty} K(u) du = 1.$$

The convolution of $K(u)$ with itself satisfies:

$$\int_{-\infty}^{\infty} (K * K)(u) du = \left(\int_{-\infty}^{\infty} K(u) du \right)^2 = 1.$$

Therefore,

$$\int_{-\infty}^{\infty} \hat{K}(u) du = 2 \int_{-\infty}^{\infty} K(u) du - \int_{-\infty}^{\infty} (K * K)(u) du = 1.$$

Thus, $\hat{K}(u)$ is normalized.

Symmetry. If $K(u)$ is symmetric, i.e., $K(u) = K(-u)$, then $(K * K)(u)$ is also symmetric. Therefore,

$$\hat{K}(-u) = 2K(-u) - (K * K)(-u) = 2K(u) - (K * K)(u) = \hat{K}(u).$$

Thus, $\hat{K}(u)$ is symmetric.

Zero First Moment. The first moment of a kernel should be zero:

$$\int_{-\infty}^{\infty} u\hat{K}(u) du = 2 \int_{-\infty}^{\infty} uK(u) du - \int_{-\infty}^{\infty} u(K * K)(u) du.$$

Since $K(u)$ is symmetric, $\int uK(u) du = 0$, and the convolution $(K * K)(u)$ is also symmetric, so $\int u(K * K)(u) du = 0$. Therefore,

$$\int_{-\infty}^{\infty} u\hat{K}(u) du = 0.$$

This confirms that $\hat{K}(u)$ has a zero first moment.

Next, note that the second moment of a kernel function, μ_2 , influences the leading term in the bias of the kernel estimator. For $\hat{K}(u)$, we have:

$$\mu_2(\hat{K}) = \int_{-\infty}^{\infty} u^2 \hat{K}(u) du = 2 \int_{-\infty}^{\infty} u^2 K(u) du - \int_{-\infty}^{\infty} u^2 (K * K)(u) du.\tag{23}$$

We know that $\int u^2 K(u) du = \mu_2(K)$. The term $\int u^2 (K * K)(u) du$ can be evaluated as follows:

$$\begin{aligned} \int u^2 (K * K)(u) du &= \int_{-\infty}^{\infty} u^2 \left(\int_{-\infty}^{\infty} K(v) K(u-v) dv \right) du \\ &= \int_{-\infty}^{\infty} K(v) \left(\int_{-\infty}^{\infty} u^2 K(u-v) du \right) dv \\ &= \int_{-\infty}^{\infty} K(v) \left(\int_{-\infty}^{\infty} (s+v)^2 K(s) ds \right) dv \\ &= \int_{-\infty}^{\infty} K(v) \left(\int s^2 K(s) ds + 2v \int s K(s) ds + v^2 \int K(s) ds \right) dv. \end{aligned}$$

Since $K(s)$ is symmetric:

$$\int s K(s) ds = 0, \quad \int s^2 K(s) ds = \mu_2(K), \quad \int K(s) ds = 1.$$

Thus, the expression simplifies to:

$$\int_{-\infty}^{\infty} K(v) (\mu_2(K) + 0 + v^2 \cdot 1) dv = \mu_2(K) \int K(v) dv + \int v^2 K(v) dv = 2\mu_2(K)$$

Thus,

$$\int u^2 (K * K)(u) du = \mu_2(K)(1) + \mu_2(K) = 2\mu_2(K).$$

Finally, returning to $\mu_2(\hat{K})$ in Eqn. 23:

$$\begin{aligned} \mu_2(\hat{K}) &= 2 \int u^2 K(u) du - \int u^2 (K * K)(u) du \\ &= 2\mu_2(K) - 2\mu_2(K) \\ &= 0. \end{aligned}$$

Implications for the bias. A classical result in statistics imply that the leading bias term of the Nadaraya-Watson estimator using kernel $K(u)$ is proportional to $\mu_2(K)h^2$:

$$\text{Bias}[\hat{m}_K(x)] \approx \frac{h^2}{2} \mu_2(K) m''(x),$$

where $m''(x)$ is the second derivative of the true regression function at point x (see, for example, (Wand & Jones, 1995)).

For the estimator using $\hat{K}(u)$, since $\mu_2(\hat{K}) = 0$, the leading bias term of order h^2 disappears. The next non-zero term in the bias expansion involves the fourth moment $\mu_4(\hat{K})$, resulting in a bias of order h^4 :

$$\text{Bias}[\hat{m}_{\hat{K}}(x)] \approx \frac{h^4}{24} \mu_4(\hat{K}) m^{(4)}(x).$$

This demonstrates that the estimator using $\hat{K}(u)$ reduces leading order bias terms that appear when $K(u)$ is used. \square

A.3 DERIVATION OF GRADIENT OF J_ω

Expand the functional $J_\omega(\mathbf{u})$ as follows:

$$J_\omega(\mathbf{u}) = \frac{1}{2} \int_{\Omega \times \Omega} \sum_{j=1}^D (u_j(x) - u_j(y))^2 w(x, y) dx dy \quad (24)$$

The gradient of J_ω with respect to \mathbf{u} is then given by:

$$\nabla_{\mathbf{u}} J_\omega(\mathbf{u}) = \left[\frac{\partial J_\omega}{\partial u_1}, \frac{\partial J_\omega}{\partial u_2}, \dots, \frac{\partial J_\omega}{\partial u_D} \right]^\top \quad (25)$$

The partial derivative $\partial J_\omega / \partial u_j$, for $j = 1, 2, \dots, D$, is defined through its dot product with an arbitrary function $h_j \in L^2(\Omega)$ as follows:

$$\begin{aligned} \frac{\partial J_\omega}{\partial u_j} \cdot h_j(x) &= \frac{d}{d\tau} J_\omega(u_j + \tau h_j) \Big|_{\tau=0} \\ &= \frac{1}{2} \left(\frac{d}{d\tau} \int_{\Omega \times \Omega} (u_j(x) - u_j(y) + \tau h_j(x) - \tau h_j(y))^2 w(x, y) dx dy \right) \Big|_{\tau=0} \\ &= \frac{1}{2} \left(\frac{d}{d\tau} \int_{\Omega \times \Omega} (u_j(x) - u_j(y) + \tau h_j(x) - \tau h_j(y))^2 w(x, y) dx dy \right) \Big|_{\tau=0} \\ &= \int_{\Omega \times \Omega} (u_j(x) - u_j(y)) (h_j(x) - h_j(y)) w(x, y) dx dy \end{aligned}$$

Applying a change of variables $(x, y) \rightarrow (y, x)$ to the second term of the above integral, we have:

$$\frac{\partial J_\omega}{\partial u_j} \cdot h_j(x) = \int_{\Omega} (u_j(x) - u_j(y)) h_j(x) (w(x, y) + w(y, x)) dy$$

Thus, the Frechet derivative of J_ω with respect to u_j is given by:

$$\frac{\partial J_\omega}{\partial u_j} = \int_{\Omega} (u_j(x) - u_j(y)) (k(x, y) + k(y, x)) dy, \quad (26)$$

which then gives the desired gradient with $w(x, y) \leftarrow w(x, y) + w(y, x)$ (Nguyen et al., 2023).

A.4 EQUIVALENCE OF SELF-ATTENTION AND NADARAYA-WATSON ESTIMATOR

We establish the relationship between self-attention, as defined in Eqn. 1, and non-parametric regression following the approaches of (Nguyen et al., 2022; Han et al., 2024; Nielsen et al., 2024). To begin, let us assume that the key and value vectors $\{\mathbf{k}_j, \mathbf{v}_j\}_{j \in [N]}$ are generated by the following data process:

$$\mathbf{v} = f(\mathbf{k}) + \epsilon, \quad (27)$$

where ϵ represents random noise with zero mean, i.e., $\mathbb{E}[\epsilon] = 0$, and f is the unknown function we aim to estimate. In this setup, the keys $\{\mathbf{k}_j\}_{j \in [N]}$ are independent and identically distributed (i.i.d.) samples drawn from the marginal distribution $p(\mathbf{k})$, characterizing the random design setting. We use $p(\mathbf{v}, \mathbf{k})$ to denote the joint distribution of the pairs (\mathbf{v}, \mathbf{k}) generated by the process described in Eqn. 27. For a new query \mathbf{q} , our goal is to estimate the function $f(\mathbf{q})$.

Recall NW estimator is a non-parametric estimator of the unknown f at any given query \mathbf{q} described by

$$f(\mathbf{k}) = \mathbb{E}[\mathbf{v} \mid \mathbf{k}] = \int_{\mathbb{R}^D} \mathbf{v} \cdot p(\mathbf{v} \mid \mathbf{k}) d\mathbf{v} = \int_{\mathbb{R}^D} \frac{\mathbf{v} \cdot p(\mathbf{v}, \mathbf{k})}{p(\mathbf{k})} d\mathbf{v},$$

where the first equality comes from the noise being zero mean, the second equality comes from the definition of conditional expectation and the final equality comes from the definition of conditional density. Eqn. 27 implies that if we can just obtain good estimates of the joint density $p(\mathbf{v}, \mathbf{k})$ and marginal density $p(\mathbf{k})$ then we can estimate the required $f(\mathbf{q})$. The Gaussian isotropic kernels with bandwidth σ are given by

$$\hat{p}_\sigma(\mathbf{v}, \mathbf{k}) = \frac{1}{N} \sum_{j \in [N]} \varphi_\sigma(\mathbf{v} - \mathbf{v}_j) \varphi_\sigma(\mathbf{k} - \mathbf{k}_j), \quad \hat{p}_\sigma(\mathbf{k}) = \frac{1}{N} \sum_{j \in [N]} \varphi_\sigma(\mathbf{k} - \mathbf{k}_j), \quad (28)$$

where φ_σ is the multivariate Gaussian density function with diagonal covariance matrix $\sigma^2 \mathbf{I}_D$. Given the kernel density estimators in Eqn. 28, the unknown function can be estimated as

$$\begin{aligned} \hat{f}_\sigma(\mathbf{k}) &= \int_{\mathbb{R}^D} \frac{\mathbf{v} \cdot \hat{p}_\sigma(\mathbf{v}, \mathbf{k})}{\hat{p}_\sigma(\mathbf{k})} d\mathbf{v} = \int_{\mathbb{R}^D} \frac{\mathbf{v} \cdot \sum_{j \in [N]} \varphi_\sigma(\mathbf{v} - \mathbf{v}_j) \varphi_\sigma(\mathbf{k} - \mathbf{k}_j)}{\sum_{j \in [N]} \varphi_\sigma(\mathbf{k} - \mathbf{k}_j)} d\mathbf{v} \\ &= \frac{\sum_{j \in [N]} \varphi_\sigma(\mathbf{k} - \mathbf{k}_j) \int \mathbf{v} \cdot \varphi_\sigma(\mathbf{v} - \mathbf{v}_j) d\mathbf{v}}{\sum_{j \in [N]} \varphi_\sigma(\mathbf{k} - \mathbf{k}_j)} = \frac{\sum_{j \in [N]} \mathbf{v}_j \varphi_\sigma(\mathbf{k} - \mathbf{k}_j)}{\sum_{j \in [N]} \varphi_\sigma(\mathbf{k} - \mathbf{k}_j)}. \end{aligned}$$

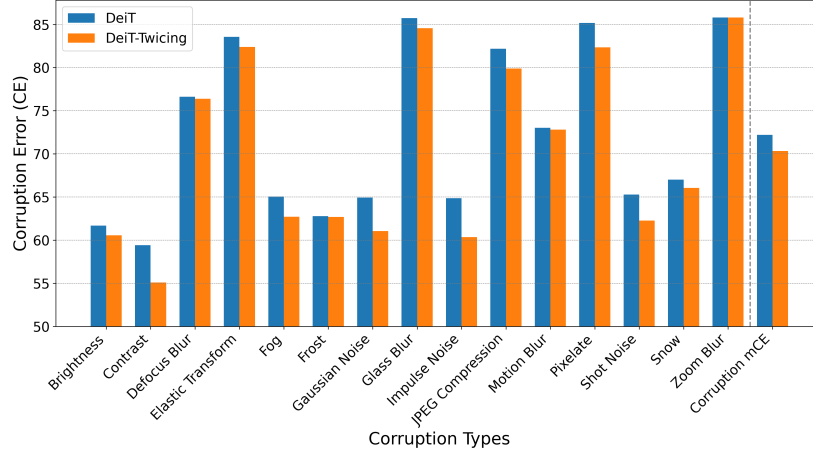


Figure 4: ImageNet-C corruption error (CE) (\downarrow) and mean CE (mCE) (\downarrow) comparison of our model and DeiT across all corruption types. Our model consistently outperforms DeiT.

Then, using the definition of the Gaussian isotropic kernel and evaluating the estimated function at \mathbf{q}_i we have

$$\begin{aligned}
 \hat{f}(\mathbf{q}_i) &= \frac{\sum_j^N \mathbf{v}_j \exp(-\|\mathbf{q}_i - \mathbf{k}_j\|^2/2\sigma^2)}{\sum_j^N \exp(-\|\mathbf{q}_i - \mathbf{k}_j\|^2/2\sigma^2)} \\
 &= \frac{\sum_j^N \mathbf{v}_j \exp[-(\|\mathbf{q}_i\|^2 + \|\mathbf{k}_j\|^2)/2\sigma^2] \exp(\mathbf{q}_i^\top \mathbf{k}_j/\sigma^2)}{\sum_j^N \exp[-(\|\mathbf{q}_i\|^2 + \|\mathbf{k}_j\|^2)/2\sigma^2] \exp(\mathbf{q}_i^\top \mathbf{k}_j/\sigma^2)} \\
 &= \frac{\sum_j^N \mathbf{v}_j \exp(\mathbf{q}_i^\top \mathbf{k}_j/\sigma^2)}{\sum_j^N \exp(\mathbf{q}_i^\top \mathbf{k}_j/\sigma^2)} = \sum_{j=1}^N \text{softmax}(\mathbf{q}_i^\top \mathbf{k}_j/\sigma^2) \mathbf{v}_j.
 \end{aligned}$$

as desired.

A.5 EQUIVALENCE BETWEEN SELF-CONVOLUTION AND SQUARE OF ATTENTION MATRIX

Let K denote the isotropic Gaussian kernel with bandwidth h . Then,

$$\begin{aligned}
 (K * K * \mathbf{v})(x) &= \int_{\Omega} K(x-t)(K * \mathbf{v})(t) dt \\
 &= \int_{\Omega} K(x-t) \int_{\Omega} K(t-y)\mathbf{v}(y) dy dt \\
 &= \int_{\Omega} \int_{\Omega} K(x-t)K(t-y) dt \mathbf{v}(y) dy \\
 &\approx \int_{\Omega} \sum_{l=1}^N K(x-l)K(l-y)\mathbf{v}(y) dy \\
 &\approx \sum_{j=1}^N \sum_{l=1}^N K(x-l)K(l-j)\mathbf{v}(j).
 \end{aligned} \tag{30}$$

Taking \mathbf{A} to be the NLM matrix whose entries are given by $\mathbf{A}_{ij} = w(i, j) = K(i - j)$, it becomes evident that Eqn. 30 can be represented as

$$(K * K * \mathbf{v})(i) \approx \sum_{j=1}^N (\mathbf{A}^2)_{ij} \mathbf{v}(j). \tag{31}$$

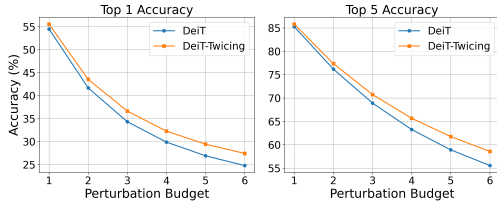


Figure 5: Top-1 and Top-5 accuracies on FGSM attack with 6 increasingly different perturbation budgets ($\times 255$).

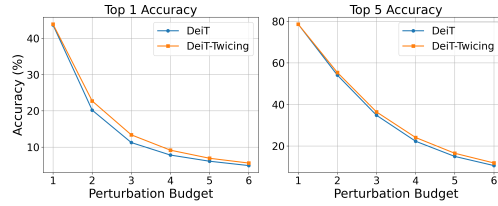


Figure 6: Top-1 and Top-5 accuracies on PGD attack with 6 increasingly different perturbation budgets ($\times 255$).

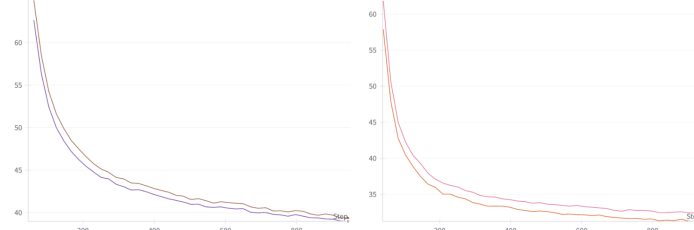


Figure 7: Validation PPL (\downarrow) training curves for baseline Transformer (higher) and Transformer-Twicing (lower). **Left:** small models (9.4M); **Right:** medium models (21M). We observe relatively faster convergence for Twicing Attention compared to standard self-attention.

B EXPERIMENTAL DETAILS AND ADDITIONAL RESULTS

B.1 WIKITEXT-103 LANGUAGE MODELLING AND WORD SWAP ATTACK

Dataset. The WikiText-103¹ dataset contains around 268K words and its training set consists of about 28K articles with 103M tokens. This corresponds to text blocks of about 3600 words. The validation set and test sets consist of 60 articles with 218K and 246K tokens respectively.

Corruption. Word Swap Text Attack² corrupts the data by substituting random words with a generic token “AAA”. We follow the setup of (Han et al., 2024) and assess models by training them on clean data before attacking only the evaluation set using a substitution rate of 4%.

Model, Optimizer & Train Specification. We adopt the training regime of (Nguyen et al., 2022). To this end, the small backbone uses 16 layers, 8 heads of dimension 16, a feedforward layer of size 2048 and an embedding dimension of 128. We use a dropout rate of 0.1. We trained with Adam using a starting learning rate of 0.00025 and cosine scheduling under default PyTorch settings. We used a batch size of 96 and trained for 120 epochs and 2000 warmup steps. The train and evaluation target lengths were set to 256.

Larger Language Modeling. To verify if Twicing Attention scales, we conduct extra language modeling on Wikitext-103 with medium sized models (21M parameters) on top of the small models (9.4M parameters) reported in the main text. The results in Figure 7 and Table 6 imply a positive answer to this matter.

Table 6: Valid/Test PPL on WikiText-103.

Model	Valid PPL	Test PPL
<i>Transformer</i> (small)	38.11	37.51
Tr.-Twicing (small)	37.12	36.69
<i>Transformer</i> (med)	31.98	26.17
Tr.-Twicing (med)	30.90	25.65

B.2 IMAGENET IMAGE CLASSIFICATION AND ADVERSARIAL ATTACK

Dataset. We use the full ImageNet dataset that contains 1.28M training images and 50K validation images. The model learns to predict the class of the input image among 1000 categories. We report the top-1 and top-5 accuracy on all experiments.

¹www.salesforce.com/products/einstein/ai-research/the-wikitext-dependency-language-modeling-dataset/

²Implementation available at github.com/QData/TextAttack

Table 7: Top-1 and Top-5 Test Accuracy on ImageNet corrupted by projected gradient descent (PGD), fast gradient sign method (FGSM), and simultaneous perturbation stochastic approximation (SPSA).

Model	ImageNet		PGD		FGSM		SPSA	
	Top 1	Top 5	Top 1	Top 5	Top 1	Top 5	Top 1	Top 5
<i>DeiT</i> (Touvron et al., 2021)	72.00	91.14	8.16	22.37	29.88	63.26	66.41	90.29
DeiT-Twicing [1-12]	72.60	<u>91.33</u>	9.15	24.10	32.28	65.67	67.12	90.53
DeiT-Twicing [7-12]	<u>72.45</u>	91.35	<u>8.67</u>	<u>22.90</u>	31.60	<u>64.79</u>	<u>66.48</u>	<u>90.52</u>
DeiT-Twicing [10-12]	<u>72.31</u>	91.24	8.66	22.58	<u>31.63</u>	64.74	66.47	90.49

Table 8: Evaluation of the performance of DeiT and DeiT-Twicing in ImageNet classification under the presence of different corruptions, using appropriate evaluation metrics for each.

Dataset	ImageNet-R	ImageNet-A	ImageNet-C	ImageNet-C (Extra)
Metric	Top 1	Top 1	mCE (\downarrow)	mCE (\downarrow)
<i>DeiT</i> (Touvron et al., 2021)	32.22	6.97	72.21	63.68
DeiT-Twicing	32.74	7.66	70.33	<u>62.46</u>
DeiT-Twicing [7-12]	<u>32.68</u>	<u>8.10</u>	69.98	62.35
DeiT-Twicing [10-12]	32.31	8.14	<u>70.25</u>	62.63

Corruption. We use attacks FGSM (Goodfellow et al., 2014) and PGD (Madry et al., 2017) with perturbation budget 4/255 while SPSA (Uesato et al., 2018) uses a perturbation budget 1/255. All attacks perturb under l_∞ norm. PGD attack uses 20 steps with step size of 0.15.

Model, Optimizer & Train Specification. The configuration follows the default DeiT tiny configuration (Touvron et al., 2021). In particular, we follow the experimental setup of (Han et al., 2024; Nguyen et al., 2022). To this end, the DeiT backbone uses 12 layers, 3 heads of dimension 64, patch size 16, feedforward layer of size 768 and embedding dimension of 192. We train using Adam with a starting learning rate of 0.0005 using cosine scheduling under default PyTorch settings, momentum of 0.9, batch size of 256, 5 warmup epochs starting from 0.000001 and 10 cooldown epochs, for an overall train run of 300 epochs. The input size is 224 and we follow the default AutoAugment policy and color jitter 0.4.

Extra results. In Figure 5 and Figure 6, we report that our model consistently outperforms the baseline across increasing six levels of severity under FGSM and PGD attacks.

B.3 OUT-OF-DISTRIBUTION ROBUSTNESS AND DATA CORRUPTION ON IMAGENET-A,R,C

ImageNet-A,R,C are benchmarks capturing a range of out-of-distribution and corrupted samples (Hendrycks et al., 2021). ImageNet-A contains real world adversarially filtered images that fool current ImageNet classifiers. ImageNet-R contains various artistic renditions of object classes from the original ImageNet. ImageNet-C consists of 15 types of algorithmically generated corruptions with 5 levels of severity. (e.g blurring, pixelation, speckle noise etc). Figure 4 shows that DeiT-Twicing (our) model outperforms DeiT baseline in all 15 main types of ImageNet-C corruptions.

B.4 ADE20K IMAGE SEGMENTATION

Experimental setup. We adopt the setup in Strudel et al. (2021). The encoder is pretrained on ImageNet-1K following the same specification described in Appendix B.2. In particular, the encoder is a DeiT-tiny backbone of 5.7M parameters pretrained for 300 epochs. After pretraining, we then attach a decoder that contains 2-layer masked transformer and finetune the full encoder-decoder model for 64 epochs on the ADE20K Zhou et al. (2019) image segmentation dataset.

C COMPUTE RESOURCES

Training. All models are trained using four NVIDIA A100 SXM4 40GB GPUs including both language and vision models.

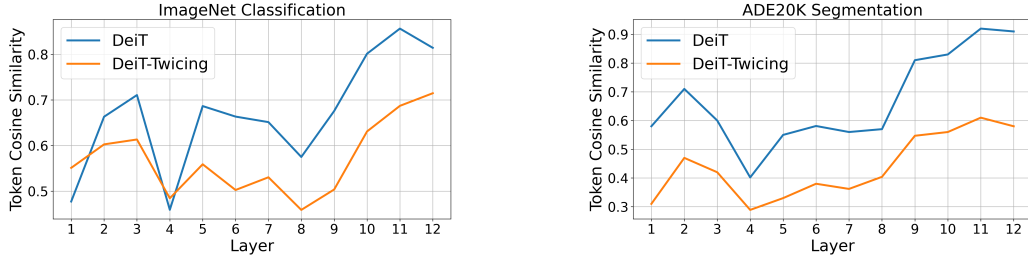


Figure 8: Comparison of average token cosine similarities across layers for DeiT and DeiT-Twicing models. Subfigure (a) uses ImageNet, while subfigure (b) evaluates ADE20K segmentation.

Evaluation. Imagenet Classification under adversarial attacks are evaluated using two NVIDIA A100 SXM4 40GB GPUs while only one of such GPUs was used to evaluate against ImageNet-A,R,C and Word Swap Attack for language modelling.

D ADDITIONAL EMPIRICAL ANALYSIS

D.1 TRAINING ANALYSIS

The trajectory of training curves for train loss, validation loss and Top-1 accuracies on ImageNet classification are shown on Figure 9.

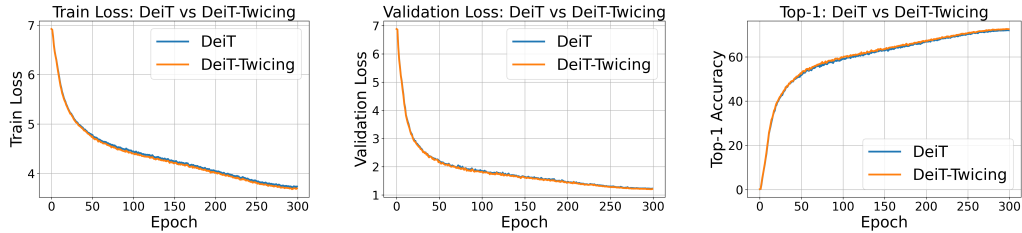


Figure 9: Comparison of Training Loss, Validation Loss, and Top-1 Accuracy

D.2 EXTRA ATTENTION HEATMAP ANALYSIS

Extending the visualizations in the main text, Figure 10 illustrates how attention heatmaps evolve from early to late layers for DeiT and DeiT-Twicing models given the input images. In Figure 11, we provide 12 more examples to show that when employed Twicing Attention, DeiT-Twicing is usually more accurate to recognize objects in images and shows substantially better expressive power by capturing more meaningful parts of objects without missing target. We also show the layer-wise over-smoothing analysis on both ImageNet classification and ADE20K image segmentation in Figure 8. We observe that in both cases, average token cosine similarities with Twicing Attention grow slower than those with standard self-attention, once again validating our theoretical findings.

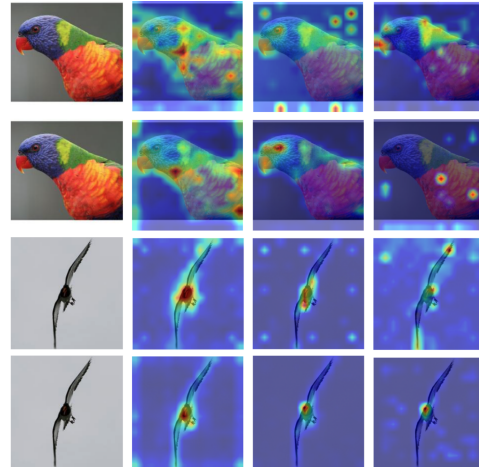


Figure 10: Evolution of attention heatmaps from early to late layers. **Odd rows:** DeiT-Twicing; **Even rows:** DeiT.

E ABLATION STUDIES

Since our proposed method does not require any additional parameters nor learnable, neither tunable, we only study the layer placement for Twicing Attention. Table 7 demonstrates 3 different layer

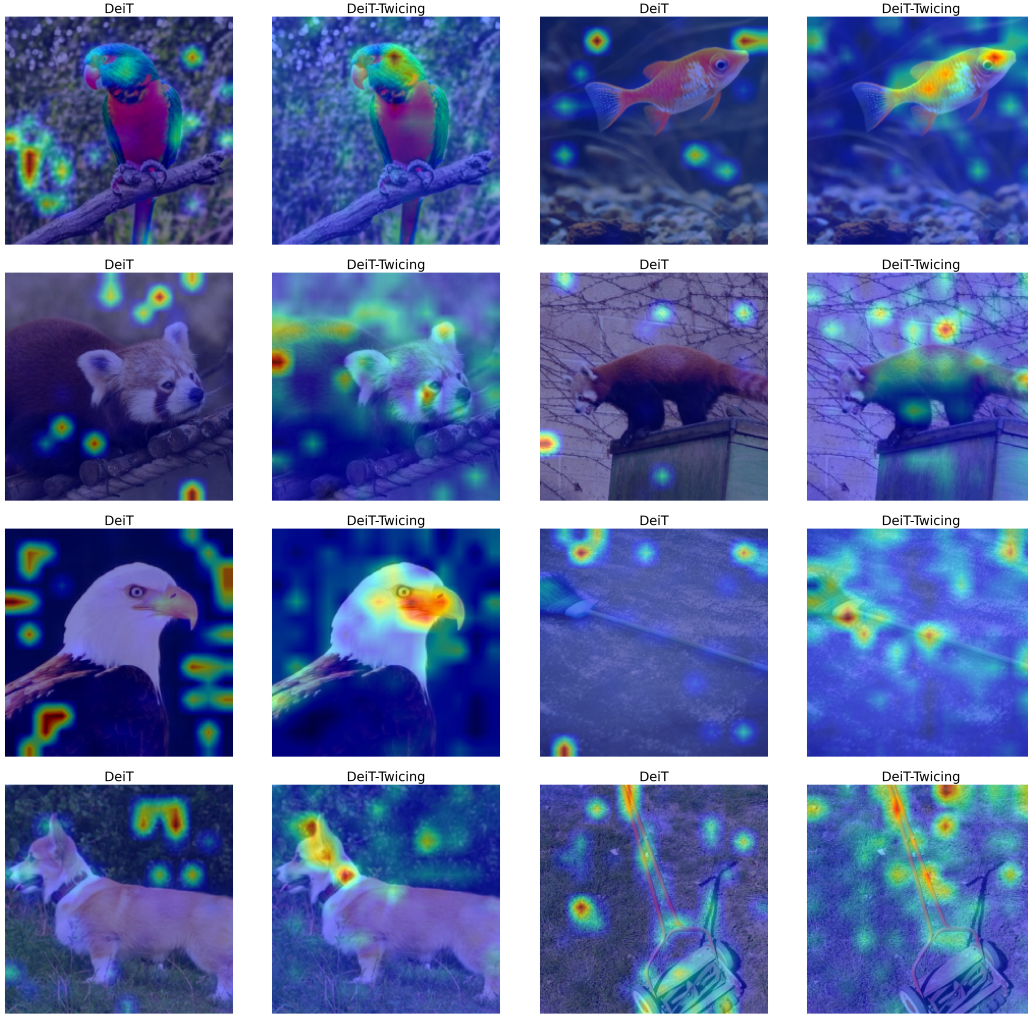


Figure 11: More examples showing how Twicing Attention is capable of retaining model’s expressive power. The DeiT baseline model frequently collapses the entire image into the background, particularly when the background occupies a significant portion of the image, making it challenging to distinguish object details. Only in few cases, such as the example in bottom right, trying to capture more information was not as successful while still being highly competitive.

placements of Twicing Attention - 1 to 12 (full), 7 to 12 (last six), and 10 to 12 (last three). We find that as long as Twicing Attention is placed starting from later layer till the end, the performance improvements are almost always proportional to the number of layers employing Twicing Attention. In Table 8, however, we observe that this proportionality does not happen in general since all three types of layer placements lead to good results in different categories, but all beating the baseline by notable margins. We also find that putting Twicing Attention only in few initial layers may not offer significant overall improvements.